Pressure Transient Analysis of a Well Penetrating a Filled Cavity in Naturally Fractured Carbonate Reservoirs

5 authors, including:

Zhaoqin Huang
China University of Petroleum, Qingdao, China
52 PUBLICATIONS   **188** CITATIONS

Yu-Shu Wu
Colorado School of Mines
276 PUBLICATIONS   **3,397** CITATIONS

Some of the authors of this publication are also working on these related projects:

Project

An efficient numerical simulation for discrete fracture model based on mixed multi-scale finite element method View project

Pressure transient analysis of a well penetrating a filled cavity in naturally fractured carbonate reservoirs

Bo Gao [a], Zhao-Qin Huang [a,b,*], Jun Yao [a], Xin-Rui Lv [c], Yu-Shu Wu [b]

[a] China University of Petroleum (East China), Qingdao 266580, China
[b] Colorado School of Mines, Golden 80401, USA
[c] Research Institute of Petroleum Exploration and Development, Sinopec, Beijing 100083 China

ABSTRACT

Naturally fractured carbonate reservoirs have been discovered in many oilfields around the world and are characteristic of a complex, heterogeneous porosity system. The presence of large-scale cavities will have a noticeable effect on the transient pressure behavior, especially, when a well is drilled through them. The cavities are usually filled with loose materials, such as gravel, sand, and mud, due to the physical or chemical processes. Therefore fluid flow in a filled cavity may range from low-velocity Darcy flow to high-velocity non-Darcy flow. It is necessary to incorporate cavity filling effect in the type curve matching for flow behavior in fractured carbonate reservoirs. The objective of this work is to develop an efficient well testing model to analyze and interpret the transient pressure responses observed in a naturally fractured carbonate reservoir, in which a well is drilled through a filled cavity. To this end, a radial composite reservoir model including the inner and outer regions with different characteristics is proposed. The inner region is a filled cavity with a well drilled into. The outer region, a naturally fractured reservoir, is considered as a dual-porosity model in this work. The Barree-Conway model, initially proposed for a proppant-packed fracture, is applied to simulate the non-Darcy flow in the inner region. The corresponding mathematical model is developed, and a numerical solution is then obtained based on the finite difference method, which is further verified by the analytical solution under simplified flow condition. Several standard log-log type curves are provided to reveal the flow characteristics. The flow process is shown to have six flow stages in general. Subsequently, sensitivity analyses of the type curves are carried out. The calculated results show that the characteristics of the well testing type curves are influenced significantly by non-Darcy coefficients, the size of the filled cavity, and the petrophysic property ratio between inner and outer areas. Finally, the proposed model is applied to analyze and interpret two field testing examples.

© 2016 Elsevier B.V. All rights reserved.

1. Introduction

In the past decade, naturally fractured carbonate reservoirs have been discovered and developed in China (Kang et al., 2005; Li, 2013; Li, 2013; Yao et al., 2010). This kind of carbonate reservoir commonly has complex pore structures and presents special challenges not found in sandstone reservoirs (Camacho-Velazquez et al., 2005; Huang et al., 2010; Popov et al., 2009a). There are three types of pores in naturally fractured carbonate reservoirs, i.e., matrix, fractures and vugs (Huang et al., 2013, 2011; Popov et al., 2009b). As observed in the outcrops of Tahe and Tarim oilfields in west China, however, some large cavities also exist in formations (as shown in Fig. 1). The sizes of these cavities may range from several meters even to tens of meters. The recent work indicates that fractured-cavity reservoirs are the major type in Tahe oilfield (Li, 2012), and there are a number of wells drilled in large cavities, which can be identified by string of beads-like seismic reflection structures and abnormal wave resistance (Li, 2012; 2013).

The transient pressure behaviors in naturally fractured carbonate reservoirs are very different from that in the conventional sandstone (Camacho-Velazquez et al., 2005; Jia et al., 2013; Wu et al., 2011a; Yang et al., 2005). If a well is drilled into a cavity, the corresponding well testing response will be more complicated. In the previous works, cavities and large-scale vugs are usually considered as voids of free-fluid flow regions, in which the Stokes equation is applied to describe the fluid flow (Arbogast and Gomez, 2009; Arbogast and Lehr, 2006; Peng et al., 2009). And then the main challenge of fluid flow modeling focuses on the coupling of free flow with porous flow (Gulbransen et al., 2010; Huang et al.,

* Corresponding author at: Colorado School of Mines, Golden 80401, USA.
E-mail address: huangzhqin@gmail.com (Z.-Q. Huang).

Nomenclature

A_1	undetermined coefficient in the analytical solution
B_i	undetermined coefficient in the analytical solution, $i=1,2$
B	volume factor, m^3/m^3
C	wellbore storage coefficient, m^3/Pa
C_i	total compressibility, $i=m,f,c,1/Pa$
I_0	the first kind of 0-order imaginary argument Bessel functions
I_1	the first kind of 1-order imaginary argument Bessel functions
K_0	the second kind of 0-order imaginary argument Bessel functions
K_1	the second kind of 1-order imaginary argument Bessel functions
a_{ij}	element of the coefficient matrix in the analytical solution, $i,j=1,2,3$
h	formation thickness, m
k_i	Darcy permeability of matrix, fracture and the filling cavity, $i=m,f,c$, μm^2
k_{min}	the minimum permeability at high velocity
k_{mr}	The minimum permeability ratio, k_{min}/k
p_i	fluid pressure, $i=m,f,c$, Pa
p_w	bottom hole pressure, Pa
∇p	pressure gradient
q	flow rate at wellhead, m^3/s
r_w	wellbore radius, m
r_c	radius of the filling cavity, m
r_e	drainage radius, m
s	skin factor
t	time, s
$\mathbf{v}$	fluid flow velocity, m/s
z	Laplace space variable

Greek letters

α	inter-porosity flow coefficient
γ	permeability ratio of the two regions
δ_N	modified high-velocity non-Darcy coefficient
δ	dimensionless modified high-velocity non-Darcy coefficient
η	diffusivity ratio between the two regions
λ	inter-porosity flow shape factor
μ	dynamic viscosity of the fluid, Pa·s
ρ	the fluid density, kg/m^3
τ	the inverse of characteristic length, 1/m
τ_D	dimensionless characteristic length
ϕ_i	porosity, $i=m,f,c$
ω	elastic storage ratio

Dimensionless parameters

C_D	dimensionless wellbore storage coefficient
p_{iD}	dimensionless pressure, $i=m,f,c$
p_{wD}	dimensionless wellbore pressure
$\tilde{p}_{iD}$	dimensionless pressure in Laplace space, $i=m,f,c$
q_{wD}	dimensionless production
r_D	dimensionless radius
t_D	dimensionless time

Superscript

n	the previous time step
n+1	the current time step

Subscript

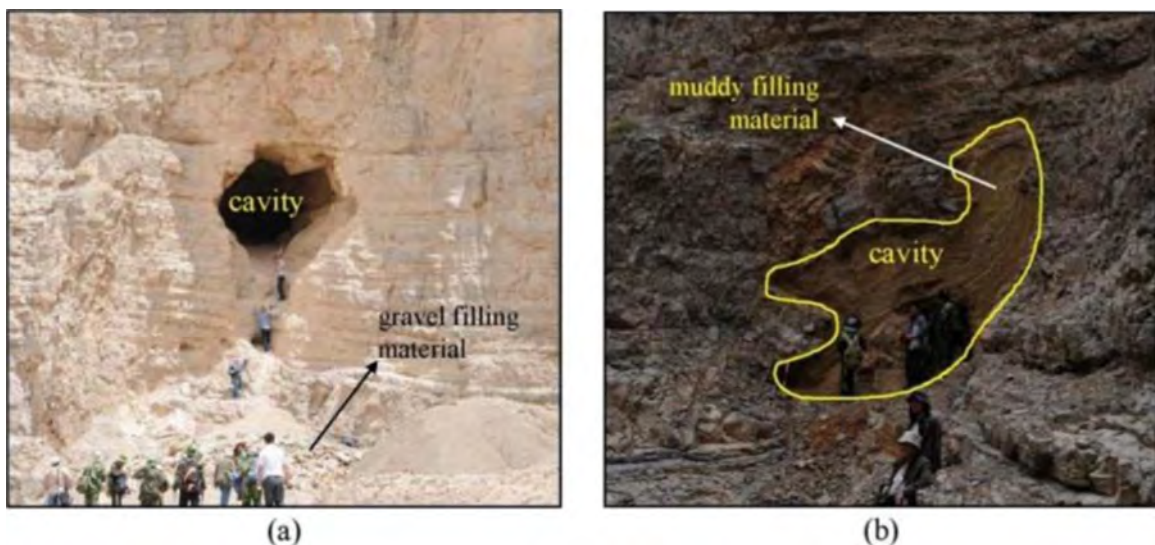|	
c	cavity
f	fractured system
m	matrix

Fig. 1. Typical outcrops of Tahe and Tarim oilfields in west China.

2011, 2010; Peng et al., 2009; Popov et al., 2009a, 2009b). The corresponding modeling results indicate that the cavities or vugs can be considered as some equipotential bodies, in which the fluid pressure is equal due to the infinite permeability. Based on this point, Liu and Wang (2012) and Yang et al. (2011) developed a simplified composite well testing model, in which the cavity is treated as an equipotential body and the outer fractured region is modelled by a dual-porosity model. Cheng et al. (2009) has

proposed a similar model in which the cavity is considered as an expanded wellbore.

However, the cavities are commonly filled with loose material, such as sand, gravel and mud (Popov et al., 2009a, 2009b), as illustrated in Fig. 1. Recently, Hu et al. (2014) and Zhang et al. (2012) studied the cavity filling characteristics based on the outcrops in northern Tarim basin and the well logs of Tahe oilfield. The results indicate that the effects of cavity filling can play a crucial role in the overall response of the reservoirs. To this end, Zhang et al. (2009) developed a well test interpretation model for naturally fractured reservoir considering a well drilled in a large cavity. In their flow model, the cavity was treated as a Darcy flow region with higher permeability than the outer porous zone. Nevertheless, they did not make further analysis of the cavity filling characterization and the corresponding effects on the transient pressure behavior in fractured reservoirs. Moreover, the filling material may be very different as mentioned above, and the dimensions of the loose material particles may range from millimeter scale to centimeter scale even meter scale. As a result, the fluid flow regime in filled cavities may range from low-velocity Darcy flow to high-velocity non-Darcy flow dependent on the filling characteristics.

The effects of high-velocity, non-Darcy flow in porous media have been investigated by using Forchheimer equation (Forchheimer, 1901) for decades (Evans et al., 1987; Huang and Ayoub, 2008; Wu, 2001; Ye et al., 2014). However, the Forchheimer equation has been found to be inadequate for modeling the non-Darcy phenomena over the entire flow velocity range (Barree and Conway, 2009, 2004; Huang and Ayoub, 2008; Ranjith and Viete, 2011). Furthermore, when we consider non-Darcy flow in a filled cavity, it is not convenient to apply the Forchheimer equation because its non-Darcy coefficient is not directly related to the cavity filling characteristics, such as the mean equivalent diameter of the filled particles. Recently, Barree and Conway (2009, 2004) developed a new physical-based model for describing the non-Darcy flow based on experimental and field data. This model has been applied to the single- and multi-phase non-Darcy flow analysis in porous media (Al-Otaibi and Wu, 2010; Wu et al., 2011b; Zhang and Yang, 2014a, 2014b). The further laboratory researches and analyses (Lai et al., 2012; Lopez-Hernandez, 2007) indicate that the Barree-Conway model can describe the non-Darcy flow behavior from low to high flow rates. Moreover, the Barree-Conway model was proposed for the proppant-packed hydraulic fracture initially so a characteristic length parameter of the filled particles exists apparently in the model. From this point of view, it is convenient and reasonable to use the Barree-Conway model to consider the cavity filling effects.

The objective of this work is to develop an efficient well testing analysis model, which is suitable for naturally fractured reservoirs with a well drilled into a large-scale cavity. We propose a composite reservoir model: (1) the filled cavity is treated as the inner region, in which a well locates at the center and the Barree-Conway model is applied to describe the fluid flow; (2) the outer region consists of naturally fractured porous media, in which the dual-porosity model is applied. This paper is organized as follows. The physical model and the corresponding mathematical well testing model are developed for the composite reservoir in Section 2. Then in Section 3, an efficient finite difference numerical scheme is applied to solve this model. The transient pressure curves and the corresponding flow characteristics are provided and the effects of some key parameters are discussed. As examples of model validation and application, two field cases are studied based on the proposed model in Section 4. Finally, several key remarks are concluded in Section 5.

2. Physical concept and mathematical model

2.1. Physical concept

The carbonate reservoir in Tahe and Tarim oilfields of China is a typical example of reservoirs composed of matrix, fracture and vug systems, called as naturally fractured vuggy carbonate reservoir. Typical outcrops in Tahe and Tarim oilfields are shown in Fig. 1. Fig. 2 shows the physical schematic model of a well drilled into a filled cavity within a fractured carbonate reservoir. As shown in Figs. 2-b and 2-c, the physical model is divided into two disparate parts: one is the interior region, i.e., the filled cavity; and the other is the outer region, i.e., the naturally fractured reservoir. In the outer part, the vug system is usually connected with fracture
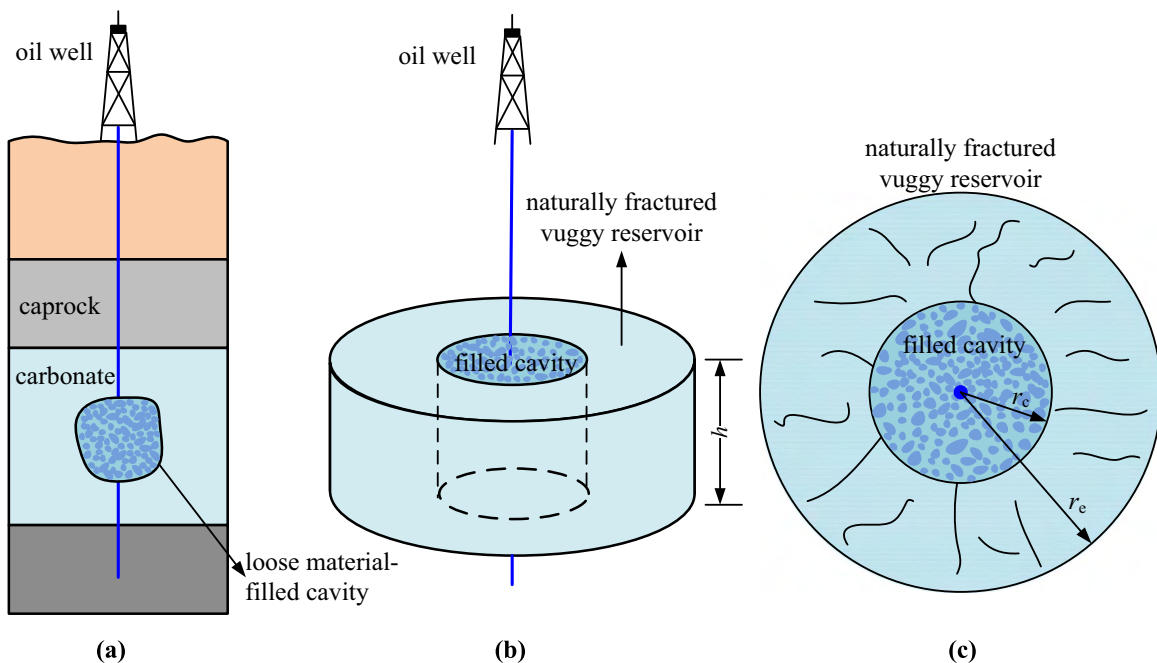

Fig. 2. Schematic of a well drilled into a filled cavity within naturally fractured reservoir (a), and its corresponding 3 – D physical model (b) and areal 2 – D physical model (c).

system, forming the main pathway for the global flow. Therefore, the whole outer region is treated as a conventional double-porosity model ([Warren and Root, 1963](#)) in this work. Moreover, the following assumptions are made for the physical model:

1. The well produces oil at a fixed volumetric rate and the reservoir has a uniform pressure distribution before production.
2. The Barree-Conway model is applied to describe the non-Darcy flow in the filled cavity (i.e. the interior region). The outer region, i.e. the fractured reservoir, is a double porosity model. The fracture-vug system is the main pathway in which linear Darcy flow model is applied, and the matrix system is only regarded as the source providing fluid to the fracture-vug system.
3. Both fluid and rock are lightly compressible with constant compressibility coefficients.
4. Gravity is neglected and no chemical or physical reactions happen, and the isothermal flow process is assumed.
5. Both the top and bottom boundaries of the reservoir are closed or impermeable.

2.2. Dimensionless mathematical model

The original mathematical model is shown in Appendix A. In order to obtain the dimensionless one, a group of dimensionless parameters should be defined first and then substituted into the previous mathematical equations. Definitions of the dimensionless parameters are listed in [Table 1](#). The last three dimensionless parameters, as well as minimum permeability ratio k_{mr}, are of great significance in this study. We will explore their influences on bottom hole pressure response, together with their practical meanings in [Section 3](#). The dimensionless mathematical model will be written as follows:

1. Non-Darcy flow region: $1 < r_D < r_{cD}$

$$\eta\gamma\frac{\partial p_{cD}}{\partial t_D} - \frac{1}{r_D}\frac{\partial}{\partial r_D}\left(r_D\delta\frac{\partial p_{cD}}{\partial r_D}\right) = 0 \tag{1}$$

2. Darcy flow region: $r_{cD} < r_D < r_{eD}$

$$\begin{cases} \omega\frac{\partial p_{fD}}{\partial t_D} - \frac{1}{r_D}\frac{\partial}{\partial r_D}\left(r_D\frac{\partial p_{fD}}{\partial r_D}\right) + \lambda\left(p_{fD} - p_{mD}\right) = 0 \\ (1-\omega)\frac{\partial p_{mD}}{\partial t_D} - \lambda\left(p_{fD} - p_{mD}\right) = 0 \end{cases} \tag{2}$$

3. Initial condition

$$p_{cD}(r_D, 0) = p_{fD}(r_D, 0) = p_{mD}(r_D, 0) = 0 \tag{3}$$

Table 1.
Dimensionless parameters.

Parameters	Definitions
Dimensionless radius, r_D	$r_D = r/(r_w e^{-s})$
Dimensionless time, t_D	$t_D = k_f t/\left[\left(\phi_m c_m + \phi_f c_f\right)\mu r_w^2\right]$
Dimensionless pressure, p_{iD}	$p_{iD} = 2\pi k_f h(p_0 - p_i)/qB\mu \quad (i = m, \ f, \ c)$
Dimensionless wellbore storage coefficient, C_D	$C_D = C/2\pi h r_w^2 \phi_c c_c$
Fluid storage capacitance coefficient, ω	$\omega = \phi_f c_f/(\phi_m c_m + \phi_f c_f)$
Inter-porosity flow factor, λ	$\lambda = \alpha(k_m/k_f)r_w^2$
Dimensionless characteristic length, τ_D	$\tau_D = \rho qB/2\pi h\mu r_w e^{-s}$
Diffusivity ratio between the two regions, η	$\eta = \phi_c c_c/(\phi_m c_m + \phi_f c_f)$
Ratio of the permeability between two regions, γ	$\gamma = k_f/k_c$

4. Inner boundary condition

$$\begin{cases} C_D\frac{dp_{wD}}{dt_D} - \delta\frac{\partial p_{cD}}{\partial r_D}\Bigg|_{r_D=1} = 1 \\ p_{wD} = \left(p_{cD} - s\delta\frac{\partial p_{cD}}{\partial r_D}\right)\Bigg|_{r_D=1} \end{cases} \tag{4}$$

5. Coupling interface conditions

$$\begin{cases} p_{cD} = p_{fD} \\ \delta\frac{\partial p_{cD}}{\partial r_D} = \gamma\frac{\partial p_{fD}}{\partial r_D}, \quad \text{at } r_D = r_{cD} \end{cases} \tag{5}$$

6. Outer boundary condition

$$\begin{cases} \frac{\partial p_{fD}}{\partial r_D}\Bigg|_{r=r_{eD}} = 0 & \text{closed boundary } r = r_{eD} \\ p_{fD}\big|_{r=r_{eD}} = p_{mD}\big|_{r=r_{eD}} = 0 & \text{constant pressure boundary } r \\ & \qquad = r_{eD} \end{cases} \tag{6}$$

where r_{cD} is the interface between two regions; p_{wD} is dimensionless wellbore pressure; δ is dimensionless modified high-velocity coefficient and given as:

$$\delta = k_{mr} + \frac{1 - k_{mr}}{1 + \tau_D(q_{rD}/r_D)} \tag{7}$$

Here, q_{rD} is the dimensionless production rate and the following is satisfied.

$$\frac{q_{rD}}{r_D} = \frac{1}{2\tau_D}\left[1 + k_{mr}\tau_D\frac{dp_{cD}}{dr_D} + \sqrt{\left(1 + k_{mr}\tau_D\frac{dp_{cD}}{dr_D}\right)^2 - 4\tau_D\frac{dp_{cD}}{dr_D}}\right] \tag{8}$$

Then, δ can be evaluated by using [Eq. (7)](#).

3. Type curves and analysis

3.1. Verification of the numerical solution

The above mathematical model is strong non-linear, so it is difficult to get an analytical solution. Therefore, numerical solution is preferred in this work. Before analysing the well testing curves obtained numerically, the numerical method and code in this paper are verified by two ways. The first is using Li's data ([Li et al., 2013](#)) of homogeneous reservoir as reference to show our non-Darcy solution method is right. Secondly, analytical solution of a composite radial reservoir, in which Darcy flow controls the whole region, is used to check the numerical method and code. The numerical solution and analytical solution processes are shown in [Appendix B](#) detailedly.

Li has studied the Barree-Convey model in homogeneous reservoir and compared it with conditional Forchheimer non-Darcy equation. The reference solution shown in [Fig. 3](#) is one of Li's solution data sets which has been published. We first use the non-Darcy part of our model to match it. The dimensionless parameters are:

$$C_D e^{2s} = 100, \quad k_{mr} = 0.1, \quad \tau_D = 3.0, \quad r_{cD} = 5000$$

Obviously, the compared result indicates that the mathematical model and numerical method of the non-Darcy part are valid.

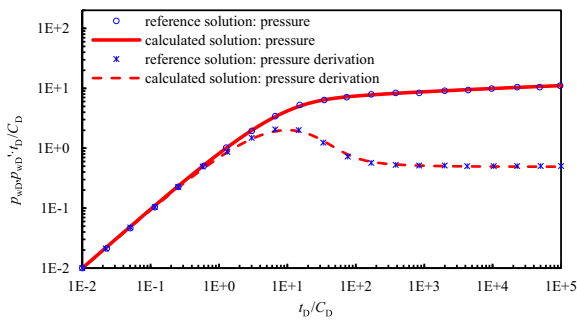Next in the second verification, we also consider a composite

Fig. 3. Comparison of reference solution by Li and calculated solution in this work.

Table 2.
Dimensionless parameters.

| Parameters	Value
Minimum permeability, k_{mr}	0.01
Dimensionless characteristic length, τ_D	10
Dimensionless radius of the filling cavity, r_{cD}	40
Ratio of the permeability of fracture to that of the filling cavity, γ	0.01
Diffusivity ratio between inner and outer part, η	5
Capacitance coefficient, ω	0.2
Fracture–Matrix inter-porosity coefficient, λe^{-2s}	10^{-6}
Dimensionless wellbore storage coefficient, $C_D e^{2s}$	10^0
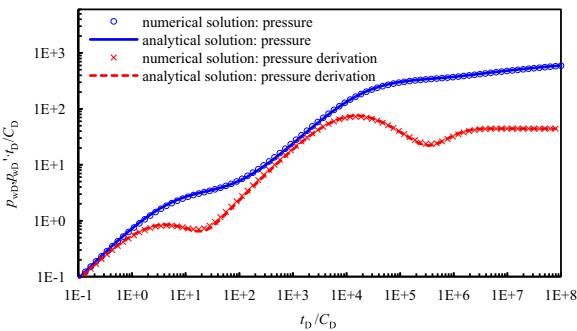
Fig. 4. Well testing curves for comparison between analytical and numerical solutions.

radial reservoir which consists two regions: the inner filled cavity which is treated as single-porosity media; the outer naturally fractured reservoir regarded as double-porosity media. The fluid flows in both regions are assumed to satisfy Darcy's law. In order to obtain this analytical solution, the Barree-Conway non-Darcy flow model used in the interior region will be reduced to Darcy flow model by setting $k_{mr}=0$ and $\tau \rightarrow \infty$. The derivation of the analytical solution is shown in detail in Appendix B.2. The Laplace space solution (B.12) is inverted by using the Stehfest algorithm (Stehfest, 1970). The dimensionless parameters listed in Table 2 are applied in this verification except that the minimum permeability and dimensionless characteristic length are neglected in the numerical solution (non-Darcy effect is not taken into considered in order to make a comparison with analytical solution), and the comparison between the numerical and analytical solutions is shown in Fig. 4. The compared results indicate the numerical solutions are in excellent agreement with the analytical ones.

3.2. Type curves

In well testing analysis, type curves are those graphic plots using analytical or numerical solutions to flow equations under specific initial conditions, boundary conditions and geometry of the interpretation model representing a reservoir-well system.
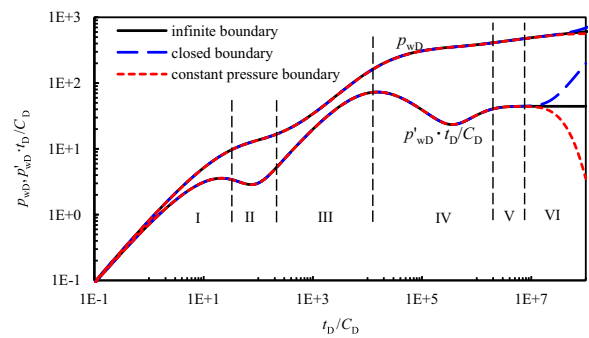

Fig. 5. Well testing type curves for different outer boundary conditions. (For interpretation of the references to color in this figure, the reader is referred to the web version of this article.)

Type curves also provide a continuous solution that incorporates the effects of the various flow stages of pressure behavior. The pressure profiles usually look identical, while the derivative curves for each situation are unique. Pressure derivative curves represent the shapes that can occur with different reservoir properties and geometries. Moreover, the pressure transients will go through several different processes as they travel, which are called flow stages or flow regimes. These flow stages depend on elapsed time and distance from the wellbore, and have characteristic pressure distributions in the reservoir.

Fig. 5 shows the dimensionless log-log well testing type curves under three different external boundaries: infinite boundary, closed boundary, and constant pressure boundary. Related dimensionless parameters are listed in Table 2. It can be divided into six flow stages:

Stage I: Wellbore storage stage. The production in this stage is dominated by the fluid initially stored in the wellbore, while formation fluid does not start flowing. Curves for pressure and its derivation are on an upward sloping line with unit-slope on a log-log plot. Besides, there is a hump exhibited on the derivative pressure curve. The type curves are controlled by dimensionless wellbore storage coefficient (C_D) and skin effect (s).

Stage II: Radial flow in the filled cavity. 3D-seismic image shows that fluid flow in collapsed karst are more radial like shapes and show radial flow. Production is dominated by the depletion of the filled cavity system. After the wellbore storage stage, the formation fluid in the cavity begins to flow into the wellbore. Therefore, wellbore pressure depletion is slow down, which makes the rate of wellbore pressure depletion decrease and the value of pressure derivative decrease accordingly; and then the system comes to the first radial flow stage. However, because of the influence of the inter-region flow differences, the pressure derivative curves in this stage may not converge to a 0.5-horizontal line. If the supply capacity of the inner filled cavity is relatively better, or the range of the cavity is larger, the stage of fluid flowing from the cavity to the wellbore will last longer; otherwise, this stage may be merged by stage I, i.e., wellbore storage stage, thus leading to a higher wellbore storage coefficient. In this stage, the type curves are controlled by the dimensionless radius and the supply capacity of the filled cavity.

Stage III: Fracture system flow from the outer region to the inner region. Production is dominated by the depletion of both the cavity (inner region) and the fracture system (outer region). After the pressure wave propagates to the boundary of the filled cavity, the fracture system in the outer region will compensate the fluid losses of the inner region. But due to the poorer physical properties than that in the inner area, i.e., a lower permeability, the pressure will grow up. Meanwhile, it also reflects an increasing trend on the derivative curve. Both the pressure

and its derivative curves ascend to a higher value. And the larger the difference, the sharper the type curves in this stage will be. In this stage, the type curves are controlled by the ratio of the permeability of fracture to that of the filling cavity.

Stage IV: Inter-porosity flow stage of matrix system to fracture system. Production is dominated by the depletion of the two regions, including the filled cavity, the fracture system and the matrix system. The pressure derivative curve is concave, which is a reflection of the inter-porosity flow of matrix to fracture system. Physical processes that occur during this inter-porosity flow stage are: wellbore pressure depletion is hindered due to fluid supplement from matrix system to the fracture system, which makes the rate of wellbore pressure depletion decrease and reflects a decrease value of the pressure derivative; however, the fluid supplement declines as the pressure depletion of the matrix system, thus resulting an increasing value of the pressure derivative accordingly. Therefore, the wellbore pressure derivative curve in the inter-porosity flow stage is a typical concave shape. In this stage, the type curves are controlled by inter-porosity flow factor.

Stage V: Radial flow stage of the whole system. Production is dominated by the depletion of both regions. The inter-porosity flow of matrix to fracture system showed in stage IV has stopped. The pressures of the whole system have gone up to a state of dynamic balance. It has come to a whole radial flow state, which is showed on the pressure derivative curve with a horizontal line with a non-0.5 value because of the difference of physical properties of the two regions. If the permeability of the fracture system is equal or higher than that of the filled cavity, this value may be close to 0.5 or even lower.

Stage VI: External boundary response stage. The pressure wave has arrived at the external boundary of the reservoir. Different external boundaries yield different curve shapes. As shown in Fig. 5, the blue, green and red lines denote the closed boundary, infinite boundary and constant pressure boundary, respectively. For a constant pressure boundary: pressure depletion of the reservoir caused by well production is suddenly supplemented, which makes the rate of wellbore pressure depletion slightly decrease and the value of the pressure derivative decrease accordingly; for a closed boundary: pressure depletion of the reservoir without the peripheral energy supplement is aggravated, which makes the rate of wellbore pressure depletion swiftly increase and the value of the pressure derivative increase accordingly. In this stage, the type curves are controlled by the dimensionless radius of external boundary.

Of course, the shape of the well testing curves will change with the different situations, in which different model parameters are used. This will be discussed in detail in the next.

3.3. Comparison of non-Darcy flow and Darcy flow in the filled cavity

Zhang et al. (2009) have also developed a well test model for naturally fractured carbonate reservoir considering a well drilled into a large-scale cavity, in which Darcy flow model was applied. Therefore, it is necessary to compare the fluid flow behavior of Darcy flow model to the Barree-Conway non-Darcy model, which are used in the filled cavity respectively. Related dimensionless parameters are the same as that listed in Table 2. As shown in Fig. 6, the pressure curves as well as its derivatives are in a similar tendency when different flow equations are applied. However, the bottom-hole pressure drop increases significantly in the first two flow stages when non-Darcy flow model is used. Meanwhile, the two flow stages in the inner region are relatively delayed for non-Darcy flow model. This is due to the larger flow resistance at
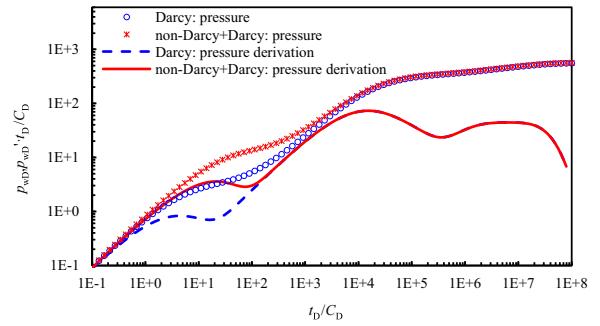

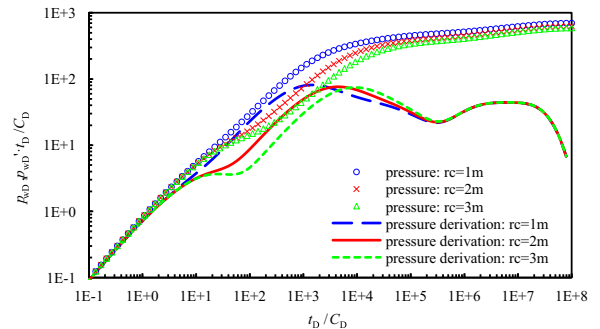**Fig. 6.** Well testing curves for different models.

Fig. 7. Well testing curves for different cavity sizes.

higher fluid flow velocity. Besides the viscosity resistance, the additional inertial term has been included in the Barree-Conway model as well as Forchheimer equation. Actually, the Barree-Conway model is a general equation to describe the entire range of flow regimes from low-velocity Darcy flow to high-velocity non-Darcy flow. So it is convenient to use this model to describe the fluid flow in a filled cavity with different filling cases.

Fig. 7 shows the effect of different size of a filled cavity on the type curves. The results indicate that a larger cavity provides enough time to represent a relatively completed flow pattern as shown in Fig. 7. In other words, the nonlinear flow in a small-radius-filling cavity will be easily overlapped by wellbore storage stage, resulting in a larger wellbore storage coefficient, especially when the cavity has a poor filling. This is the case of the research works developed by (Cheng et al., 2009; Liu and Wang, 2012; Yang et al., 2011).

3.4. Influences of non-Darcy parameters

The Barree-Conway model describes the fluid flow in a filled cavity using two non-Darcy parameters: k_{mr} and τ_D (Note that τ_D is related to adverse characteristic length). Figs. 8 and 9 show the influences of the different parameters value on the transient
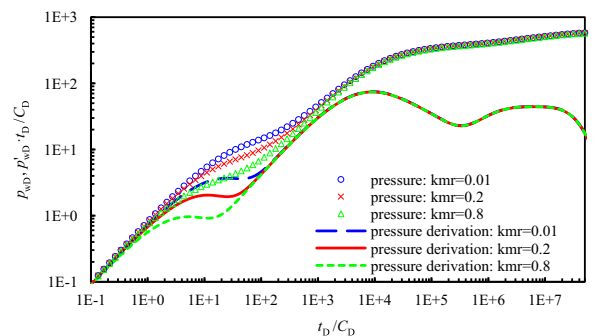

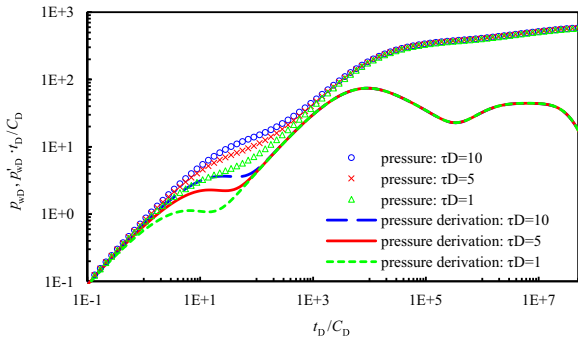**Fig. 8.** Well testing curves for different k_{mr}.

Fig. 9. Well testing curves for different τ_D.

Fig. 10. Well testing curves for different γ.

pressure behavior. Related dimensionless parameters are listed in Table 2 except the dimensionless cavity radius, which is set to 30. The results show that the bottom-hole pressure drop rises and the flow stages shift right with the decrease of k_{mr} and increase of τ_D. As a smaller k_{mr} and a larger τ_D, varying inversely with τ, represents a stronger non-Darcy effect. k_{mr} is the minimum permeability ratio related to the minimum permeability at high flow rate when non-Darcy flow occurs. Various explanations for its physical meaning have been advanced in different literature, mainly including two mechanisms, which are both associated with the pore structure (Barree and Conway, 2004).

(1) Due to the different filling materials and compaction degrees, the pore structures in a filled cavity may vary dramatically. In normal porous media flow, the fluid will accelerate through the relatively narrow pores and inversely decelerate when passing larger ones. Such repeated changes in velocity must lead to inertial losses, which are responsible for the decrease in apparent permeability associated with non-Darcy flow. Edwards et al. (1990) suggest that at higher rates, the flow will keep a better defined streamlines in the whole body, rather than become slower when entering larger pores. As a result, the inertial loses introduced by changing velocity will be minimized. The system will approach a nearly constant apparent permeability.

(2) Another exploration is that at low rate, most part of the total flow capacity is dominated by large pore channels. While as flow rate increases, the flow will divert to smaller pores successively, thus reaching a more uniform velocity distribution in the system and compensating for the inertial losses. Therefore, if the pore size ranges in a narrow scale, the inertial losses will be small accordingly. A uniform velocity distribution will be easily to be satisfied and the minimum permeability may approximate the real permeability. Inversely, the minimum permeability will be very small if the pore structure is quite complex.

So the parameter, k_{mr}, can be used to describe the complexity of the pore structure. A smaller k_{mr} represents more heterogeneous filling and compaction in a cavity, and a larger flow resistance. The characteristic length parameter, τ, is related to the mean particle diameter of the filling materials. So it can be used to describe the characteristic dimension of the filling material particles. A smaller τ represents a larger size of the filling particles. Therefore, the specific surface is smaller, and the flow rate is higher. And then, the fluid flow in a filled cavity will deviate more from linear Darcy flow.

3.5. Influences of rock properties of inner and outer regions

Fig. 10 shows well testing curves with different permeability ratios γ. Related dimensionless parameters chosen here are the
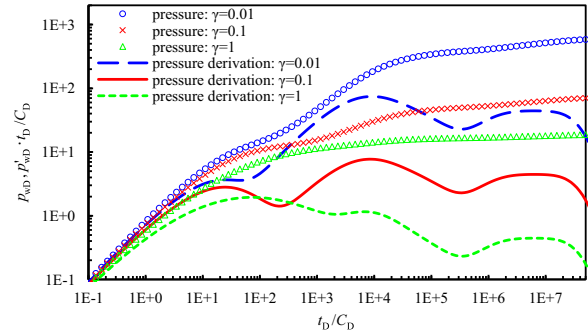
same as those in Section 3.4. $\gamma=1$ means the fracture system of the outer region has the same permeability as that of the filled cavity. In this case, the phenomenon of obvious pressure drop increases, as expounded above, does not appear due to the same permeability. Moreover, the fluid supply process from the cavity happens later. While $\gamma<1$, the smaller value of parameter γ means the larger difference of the rock properties between the two regions. The change of the bottom-hole pressure drop is more evident and the flow stages are more remarkable.

Fig. 11 shows the well testing curves with different ratios of diffusivity η between the two regions. If $\eta<1$, the supply ability of the inner region is worse than that of the outer region. Hence the pressure wave will propagate to the coupling interface between the cavity and outer region in an early stage. And there is nearly a zero pressure-change while propagating from the cavity to the outer region. Actually, the stage III of the type curve may be considered as an additional wellbore storage effect. With the increase of η, the fluid supply capacity of the filled cavity becomes better and the stage II will last longer.

4. Field case study

The derived type curves in Section 3 would be a family of specific "Geotype" curves for naturally fractured carbonate reservoirs. Our conceptual model can be used to evaluate the filling characteristics of a filled cavity, where a well drilled. In the following, we will validate our conceptual model by using two real field production well data. And then some meaningful well test interpretation results can be obtained.

4.1. Case 1

In this case, the proposed well test model is used to analyze well test data in Tahe oilfield. This is an evaluation well located in the north of Qiemo county in Xinjiang province (Yang et al., 2011). It was began to be spud in on December 4, 2006 and finished on
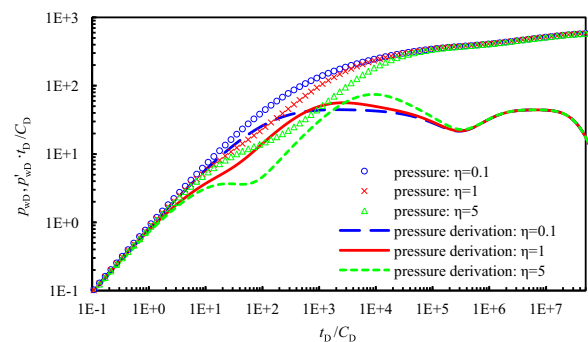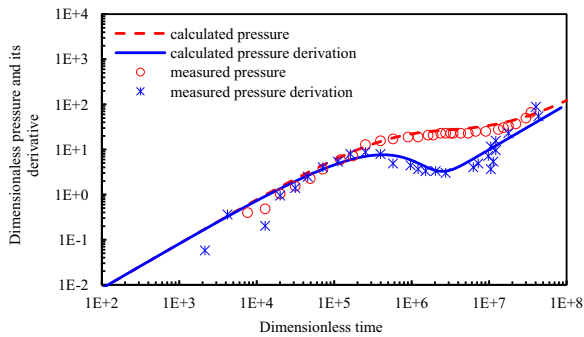

Fig. 11. Well testing curves for different η.

Fig. 12. Well testing curves in case 1.

Fig. 13. Matching curves of well testing interpretations in case 2.

April 13, 2007. The well depth is 5750 m. Drilling stem emptying and massive mud leakage indicated the well drilled in a large-scale cavity in the objective formation. Fig. 12 shows that the calculated results based on our mathematical model match the real observed data very well.

The dimensionless well test interpretation results are presented in Table 3. The minimum permeability k_{mr} is 0.01, a small value. The pore size distribution in this formation is relatively non-uniform, leading to stronger inertial losses during the flow process. Therefore, loose muddy filling materials are expected in the cavity. This has been verified by the well log information. The dimensionless characteristic length parameter τ_D is 22, which indicates that the average size of the filling material particles is relatively small (compared with that in the case 2). Both the specific surface and the flow resistance are larger. The dimensionless radius of the filled cavity is 40, which implies the scale of the filled cavity is small. At the same time, the wellbore storage coefficient is large. Hence, the cavity-flow stage (Stage II) lasts for a short time and is very easily overlapped by the wellbore storage stage (Stage I).

The parameter $\gamma > 1$ as seen in Table 3 means the permeability of the outer region is higher than that of the filled cavity. So there is supposed to show a dramatic increase in the third stage of the pressure and its derivative curve. However, there shows no obvious evidence for such a phenomenon in the early stage in Fig. 12. In the late stage, the pressure and pressure derivative go up because of confronting the closed boundary. Besides, the diffusivity ratio between the inner and outer part η equals 1, indicating that these two regions have a similar capacity to supply fluid. Therefore, a conclusion can be drawn from the above analysis: the cavity flow stage merges with the wellbore storage stage, and the well production mainly depends on the outer region rather than the filled cavity. In sum, the matching effect is desirable and the interpretation results are credible.

4.2. Case 2

In this case, an oil production well in Tarim oilfield is selected to analyze. It is a typical fractured vuggy carbonate reservoir

located in the north area of Tarim basin. During the drilling operation, the total height of drill stem empty is 14.68 m and the accumulated leak drilling fluid is 476.2 m³, which indicate the well has drilled into a cavity. Meanwhile, both the well log curves and seismic profiles show it is a typical cavity-fractured carbonate reservoir. The matching curves of well test interpretation are presented in Fig. 13. The corresponding well test interpretation results are shown in Table 4.

Fig. 13 shows a totally different result from that in the case 1. The minimum permeability k_{mr} in this case is 0.15, relatively high, which means a good compaction and that the pore size distribution is relatively uniform. So the inertial losses is small on the flow process. The dimensionless characteristic length parameter τ_D is 200, which implies the average size of the filling material particles is large and the specific surface is small, leading to a low flow resistance. The radius of the non-Darcy near-wellbore area is 190 m (Liu et al., 2014), a wide range. The cavity-flow stage (Stage II) will last for a relatively long time. The permeability ratio γ is 0.01. In other words, the permeability of the outer region is much smaller than that of the filled cavity. Therefore, the pressure and its derivative climb up when the pressure wave spreads across the boundary of the inner region, as shown in Fig. 13. The diffusivity ratio η between the two areas is large, indicating that the vicinity nearby the well has a strong capacity to deliver fluid to the wellbore. Thus it results in a longer cavity-flow stage. In addition, the wellbore storage stage still dominates in the early stage.

5. Conclusions

This research presents the well test analysis model and its solution for fractured carbonate reservoirs with a well drilled into a filled cavity. The standard type curves are provided and analyzed, and the flow model and numerical method have been applied in two field tests. The following conclusions can be drawn:

1. A cavity within a naturally fractured reservoir has important

Table 3.
Dimensionless parameters used to match field case 1.

Parameters	Value
Minimum permeability, k_{mr}	0.01
Dimensionless characteristic length, τ_D	22
Dimensionless radius of the filling cavity, r_{cD}	40
Ratio of the permeability of fracture to that of the filled cavity, γ	2
Diffusivity ratio between inner and outer part, η	1
Capacitance coefficient, ω	0.01
Fracture–Matrix inter-porosity coefficient, λe^{-2s}	10^{-6}
Dimensionless wellbore storage coefficient, $C_D e^{2s}$	1.2×10^4

Table 4.
Dimensionless parameters used to match field data in case 2.

Parameters	Value
Minimum permeability, k_{mr}	0.15
Dimensionless characteristic length, τ_D	200
Dimensionless radius of the filling cavity, r_{cD}	1900
Ratio of the permeability of fracture to that of the filling cavity, γ	0.01
Diffusivity ratio between inner and outer part, η	20
Capacitance coefficient, ω	0.01
Fracture–Matrix inter-porosity coefficient, λe^{-2s}	10^{-6}
Dimensionless wellbore storage coefficient, $C_D e^{2s}$	2.5×10^3

effect on pressure transient during well testing, especially for a filled cavity. However, the flow rate and regime differs due to different cavity filling degree, which may range from low-velocity Darcy flow to high-velocity non-Darcy flow. Our results show that the Barree-Conway model is useful and efficient to describe the flow process within a filled cavity.

2. The corresponding type curve is divided into six stages. These stages are influenced by some key parameters, such as the wellbore storage coefficient, the filling material particle size, the supply capacity of a filled cavity, the ratio of the permeability of fracture to that of the filling cavity, the inter-porosity flow factor, and the external-boundary conditions. Compared with the Darcy model, the bottom-hole pressure drop increases by using the Barree-Conway non-Darcy model.

3. k_{mr} and τ_D are the two key non-Darcy parameters to determine the shape of the well testing curve. A smaller k_{mr} represents more heterogeneous filling and compaction in a cavity, and a larger τ_D represents a higher average value of the filler's size. With the decrease of k_{mr} and increase of τ_D, non-Darcy effect becomes more obvious, thus it will result in the rise of pressure drop.

4. The permeability ratio of fractures of the outer region and the filled cave is smaller, the change of the pressure at the boundary of the inner region will be more evident and sharper. Besides, a larger inner-outer diffusivity ratio means a better supply capacity of the cavity, and a longer cave flow stage will exist.

5. Successful field data interpretation validates the effectiveness of the provided model, which demonstrated that this model could be applied to real case studies.

Acknowledgments

Appendix A

A.1. The interior region: the filled cavity

A schematic composite reservoir is depicted in Fig. 2-c. The interior region ($r_w < r < r_c$) is the filled cavity area. r_w is the wellbore radius, and r_c is the outer boundary of the cavity. The flow in the filled cavity is described by the Barree-Conway model, which will be elaborated in this Section. While the outer dual-porosity region ($r_c < r < r_e$) is the Darcy flow zone, and r_e is the radius of exterior boundary.

Based on experimental results and field observations, Barree and Conway (2004, 2009) proposed a new, physical-based model for describing non-Darcy flow in proppant fractures for both single phase and multiphase flows. The new model does not rely on the assumption of a constant permeability or a constant Forchheimer-β factor, which is given by

$$-\nabla p = \frac{\mu \mathbf{v}}{k \left[k_{mr} + \frac{(1 - k_{mr})\mu\tau}{\mu\tau + \rho |\mathbf{v}|} \right]} \quad (A.1)$$

where k is the absolute (Darcy) permeability; k_{mr} is the ratio of minimum permeability to the Darcy's permeability, i.e., k_{min}/k; μ is the dynamic viscosity of the fluid, τ is the inverse of characteristic length, and ∇p is the pressure gradient. Equation (A.1) can be simplified into Forchheimer equation if $k_{mr}=0$, or Darcy equation

if $k_{mr}=1$ or $\tau \to \infty$.

Recent laboratory studies and analyses have shown that the Barree-Conway model provides a single equation to describe the entire range of flow velocities versus pressure or potential gradient from low-velocity Darcy flow to high-velocity non-Darcy flow regimes, including those in transitional zones (Lai et al., 2012). At low flow rates, the Barree-Conway model simplifies to Darcy equation with a constant permeability k. And the Barree-Conway model also provides a plateau area at high rates, which indicates there is a minimum permeability, consistent with laboratory and finite element modeling results (Barree and Conway, 2004). Moreover, the Barree-Conway model was proposed firstly for the proppant-packed hydraulic fracture, so a characteristic length parameter of the packed particles, i.e., parameter τ, exists apparently in the model. It is intuitive and convenient to apply the Barree-Conway model to consider the filling effect of a filled cavity.

As shown in Fig. 2, considering a radial cylindrical flow system and neglecting the source and sink, the mass conservation equation in a filled cavity is given by:

$$\rho \phi_c C_c \frac{\partial p_c}{\partial t} = \frac{1}{r} \frac{\partial}{\partial r}(r \cdot \rho v) \ , \quad (r_w < r < r_c) \quad (A.2)$$

where ϕ_c is the porosity of the filled cavity, and C_c is the total compressibility of fluid and filling material in the cavity. According to the Barree-Conway model (i.e., equation (A.1)), the velocity v in equation (A.2) is written as:

$$v = \frac{k_c}{\mu} \left(k_{mr} + \frac{1 - k_{mr}}{1 + \rho v / \mu\tau} \right) \frac{\partial p_c}{\partial r} \quad (A.3)$$

Then the governing equation of the inner region in radial system can be obtained as follows:

$$\frac{\phi_c C_c \mu}{k_c} \frac{\partial p_c}{\partial t} - \frac{1}{r} \frac{\partial}{\partial r} \left(r \delta_N \frac{\partial p_c}{\partial r} \right) = 0 \quad (r_w < r < r_c) \quad (A.4)$$

where δ_N is the non-Darcy coefficient:

$$\delta_N = k_{mr} + \frac{1 - k_{mr}}{1 + \rho v / \mu\tau} \quad (A.5)$$

A.2 The outer region: naturally fractured porous media

The outer region is naturally fractured porous media, in which three porosity types (matrix, fractures, and vugs) are usually present. There are two major models have been developed to analyze the transient pressure behavior in fractured carbonate reservoirs: the dual-porosity model and the triple-porosity model (Wang et al., 2014; Wu et al., 2011a; Yang et al., 2005). The main difference between these two models is the treatment of the vugs. In the triple-porosity model, vugs are considered as a single system. In this work, we will use the dual-porosity model.

To use the dual-porosity model to study the behavior of naturally fractured reservoirs, it is required that matrix, fracture, and vug porosities be partitioned into primary and secondary porosities. In this work, the connected vugs are treated as fracture system, while the rest of the vugs can be treated as isolated vugs and included in the matrix system. And then, the whole outer region can be considered as a conventional dual-porosity model (Barenblatt et al., 1960; Warren and Root, 1963), in which the fracture system is the flow system and the matrix system is regarded as the main source. The corresponding governing equations based on Darcy's Law are given by:

$$\begin{cases} \dfrac{\phi_f C_f \mu}{k_f}\dfrac{\partial p_f}{\partial t} - \dfrac{1}{r}\dfrac{\partial}{\partial r}\left(r\dfrac{\partial p_f}{\partial r}\right) - \dfrac{\alpha k_m}{k_f}\left(p_m - p_f\right) = 0 \\ \qquad \dfrac{\phi_m C_m \mu}{k_m}\dfrac{\partial p_m}{\partial t} + \alpha\left(p_m - p_f\right) = 0 \end{cases} \quad (r_c < r < r_e)$$

(A.6)

where the subscript "c", "f", "m" represent the filled cavity, fracture and matrix system respectively. p_i (i=f, m) is pressure, ϕ_i (i=f, m) is porosity, C_i (i=f, m) is the total compressibility, k_i (i=f, m) is permeability, μ is the viscosity of fluid, and α is the inter-porosity flow coefficient.

A.3 The initial and boundary conditions

The pressure in the reservoir is uniformly distributed at the initial state:

$$p_i(r, t = 0) = p_0 \quad (i = c, f, m) \tag{A.7}$$

Two types of outer boundary conditions are expressed as:

$$\begin{cases} p_f\big|_{r=r_e} = p_0 & \text{constant pressure boundary} \\ \dfrac{\partial p_f}{\partial r}\bigg|_{r=r_e} = 0 & \text{closed boundary} \end{cases} \tag{A.8}$$

Considering the high-velocity non-Darcy flow, the inner boundary condition with the wellbore storage effect is slightly different from the conventional one. It is given as:

$$\frac{2\pi k_c h}{\mu}\left(r\delta_N\frac{\partial p_c}{\partial r}\right)\bigg|_{r=r_w} - C\frac{dp_w}{dt} = qB \tag{A.9}$$

where h is formation thickness, C is the wellbore storage coefficient, B is formation volume factor, q is flow rate at wellhead, and p_w is the bottom hole pressure. Considering the skin effect, the wellbore pressure, p_w, can be expressed as:

$$p_w = \left(p_c - sr\delta_N\frac{\partial p_c}{\partial r}\right)\bigg|_{r=r_w} \tag{A.10}$$

where s is skin factor.

Furthermore, the interface continuity conditions are imposed at $r=r_c$ in order to couple the inner and outer regions, which is given as:

$$\begin{cases} p_c = p_f \\ \delta_N\dfrac{k_c}{\mu}\dfrac{\partial p_c}{\partial r} = \dfrac{k_f}{\mu}\dfrac{\partial p_f}{\partial r}, \end{cases} \quad \text{at } r = r_c \tag{A.11}$$

Based on the dimensionless definitions shown in Table 1, the radial Barree-Conway model Eq. (A.3) can be rewritten as the following dimensionless form:

$$-\frac{dp_{cD}}{dr_D} = \frac{1}{\delta}\frac{q_{rD}}{r_D} \tag{A.12}$$

According to equations (A.12) and (7), (8) can be obtained.

Appendix B

B.1 Finite difference numerical scheme

The numerical scheme is developed in this section. Geometric sequence grids is used, and the radial coordinate is transformed into a rectangular system by using $r_D = e^x$. Then the mathematical well testing model is discretized by using the central difference scheme.

(1) Inner boundary: $i = 1$

$$\left[\frac{C_D}{\Delta t}\left(1 + \frac{s\delta_1^{n+1}}{\Delta x_1}\right) + \frac{\delta_1^{n+1}}{\Delta x_1}\right]p_{cD1}^{n+1} - \left(\frac{C_D s\delta_1^{n+1}}{\Delta t\Delta x_1} + \frac{\delta_1^{n+1}}{\Delta x_1}\right)p_{cD2}^{n+1}$$
$$= 1 + \frac{C_D}{\Delta t}\left[p_{cD1}^n - \frac{s\delta_1^{n+1}}{\Delta x_1}\left(p_{cD2}^n - p_{cD1}^n\right)\right] \tag{B.1}$$

(2) Non-Darcy region: $i = 2, 3, \dots, m$

$$\delta_{i-1/2}^{n+1}p_{cD\ i-1}^{n+1} - \left(\delta_{i-1/2}^{n+1} + \delta_{i+1/2}^{n+1} + M_i\right)p_{cD\ i}^{n+1} + \delta_{i+1/2}^{n+1}p_{cD\ i+1}^{n+1}$$
$$= -M_i p_{cD\ i}^n \tag{B.2}$$

where

$$M_i = \frac{\eta\gamma\Delta x_1^2 e^{\left[2(i-1)\Delta x_1 - 2s\right]}}{\Delta t}$$

and m is the maximum number of grids in non-Darcy region, $\Delta x_1 = \ln r_{cD}/m$ is the uniform grid length of non-Darcy region, and Δt is time step.

(3) Coupling interface boundary: $i = m + 1$

$$-\frac{\delta_{i-1}^{n+1}}{\Delta x_1}p_{cD\ i-1}^{n+1} + \left(\frac{\delta_{i-1}^{n+1}}{\Delta x_1} + \frac{\gamma}{\Delta x_2}\right)p_{cD\ i}^{n+1} - \frac{\gamma}{\Delta x_2}p_{fD\ i+1}^{n+1} = 0 \tag{B.3}$$

(4) Darcy region: $i = m + 2, m + 3, \dots, m + l$
    The fracture system:

$$p_{fD\ i-1}^{n+1} - \left(2 + E_i + F_i\right)p_{fD\ i}^{n+1} + p_{fD\ i+1}^{n+1} = -E_i p_{fD\ i}^n - F_i p_{mD\ i}^n \tag{B.4}$$

The matrix system:

$$p_{mD\ i+1}^{n+1} = \frac{\lambda\Delta t}{1 - \omega + \lambda\Delta t}p_{fD\ i}^{n+1} + \frac{1 - \omega}{1 - \omega + \lambda\Delta t}p_{mD\ i}^n \tag{B.5}$$

where

$$\begin{cases} E_i = \dfrac{\omega\Delta x_2^2 e^{2\left[m\Delta x_1 + (i-m-1)\Delta x_2 - s\right]}}{\Delta t} \\ F_i = \left(1 - \omega\right)/\left(1 - \omega + \lambda\Delta t\right)\lambda\Delta x_2^2 e^{2\left[m\Delta x_1 + (i-m-1)\Delta x_2 - s\right]} \end{cases}$$

and l is the maximum number of grids in the Darcy region; $\Delta x_1 = (\ln r_{eD} - \ln r_{cD})/l$ is the uniform grid length of Darcy region.

(5) Outer boundary: $i = m + l + 1$

$$\begin{cases} p_{fD\ i}^{n+1} = p_{mD\ i}^{n+1} = 0 & \text{for constant pressure boundary} \\ 2p_{fD\ i-1}^{n+1} - \left(2 + E_i + F_i\right)p_{fD\ i}^{n+1} & \text{for closed boundary} \\ \quad = -E_i p_{fD\ i}^n - F_i p_{mD\ i}^n \end{cases} \tag{B.6}$$

The solving process for the above non-linear system is illustrated in Fig. B.1.

B.2 Analytical solution of a simplified model

In order to obtain this analytical solution, the Barree-Conway non-Darcy flow model used in the interior region will be reduced to Darcy flow model. As mentioned above, Darcy's equation is a limiting case of the Barree-Conway model, when $k_{mr}=0$ and $\tau \to \infty$, as saw in Section A.1. Applying Laplace transformation to (Eqs (1)–6) and considering infinite boundary condition, we can get the Laplace space solution of the mathematical model, as follows:

$$\tilde{p}_{cD} = A_1 I_0\left(r_D\sqrt{z\eta\gamma}\right) + B_1 K_0\left(r_D\sqrt{z\eta\gamma}\right)\tilde{p}_{fD} = B_2 K_0\left(r_D\sqrt{zf(z)}\right)f(z)$$
$$= \frac{\omega(1 - \omega)z + \lambda}{(1 - \omega)z + \lambda} \tag{B.7}$$

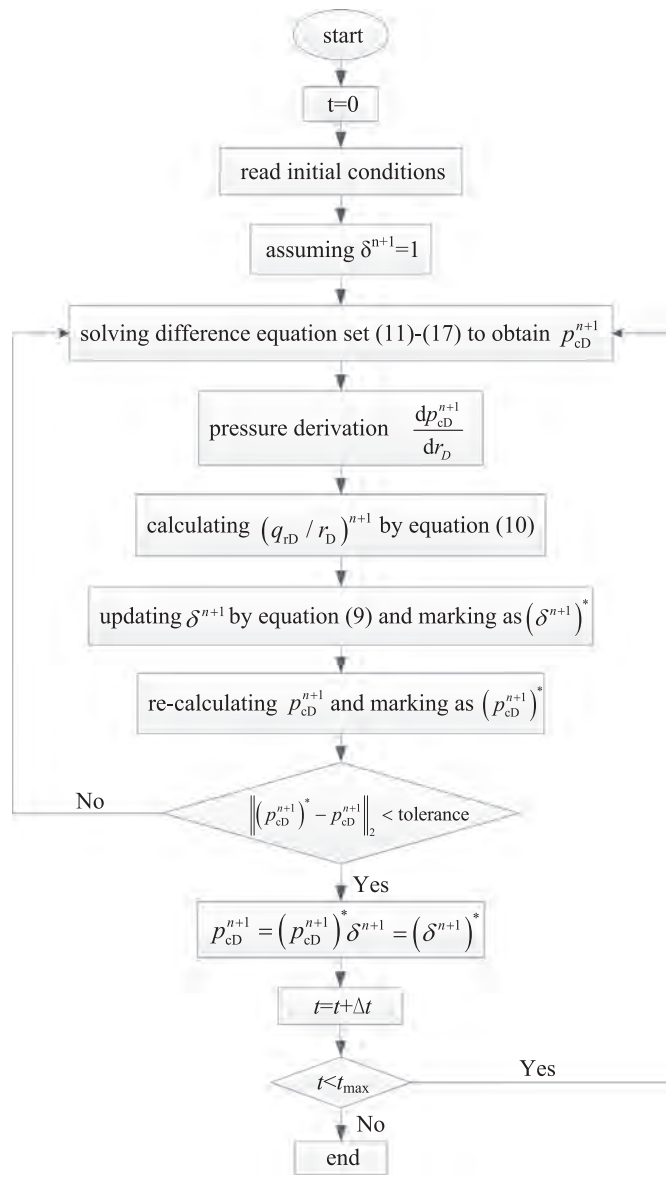where z is the Laplace variable; I_0 and K_0 are 0-order Bessel

Fig. B.1. Solution flow scheme.

functions; A_1, B_1 and B_2 are undetermined coefficients, which can be obtained by the following boundary conditions.

(1) Inner boundary condition ($r_D = 1$):

$$\frac{d\tilde{p}_{cD}}{dr_D} - \frac{C_D z^2}{C_D z^2 s + z}\tilde{p}_{cD} + \frac{1}{C_D z^2 s + z} = 0 \tag{B.8}$$

(2) Coupling interface conditions ($r_D = r_{cD}$):

$$\begin{cases} \tilde{p}_{cD} = \tilde{p}_{fD} \\ \dfrac{d\tilde{p}_{cD}}{dr_D} = \gamma \dfrac{d\tilde{p}_{fD}}{dr_D}, \quad r_D = r_{cD} \end{cases} \tag{B.9}$$

Substituting equation (B.7) to equations (B.8) and (B.9), we can get:

$$\begin{bmatrix} a_{11} & a_{12} & 0 \\ a_{21} & a_{22} & a_{23} \\ a_{31} & a_{32} & a_{33} \end{bmatrix}\begin{bmatrix} A_1 \\ B_1 \\ B_2 \end{bmatrix} = \begin{bmatrix} f_1 \\ 0 \\ 0 \end{bmatrix} \tag{B.10}$$

where

$$a_{11} = \sqrt{z\eta\gamma}\,I_1\!\left(\sqrt{z\eta\gamma}\right) - \frac{C_D z^2}{C_D z^2 s + z}I_0\!\left(\sqrt{z\eta\gamma}\right)\ a_{12}$$

$$= -\sqrt{z\eta\gamma}\,K_1\!\left(\sqrt{z\eta\gamma}\right) - \frac{C_D z^2}{C_D z^2 s + z}K_0\!\left(\sqrt{z\eta\gamma}\right)a_{21} = I_0\!\left(r_{cD}\sqrt{z\eta\gamma}\right)$$

$$a_{22} = K_0\!\left(r_{cD}\sqrt{z\eta\gamma}\right) \quad a_{23} = -K_0\!\left(r_{cD}\sqrt{zf(z)}\right)a_{31}$$

$$= \sqrt{z\eta\gamma}\,I_1\!\left(r_{cD}\sqrt{z\eta\gamma}\right) \quad a_{32} = -\sqrt{z\eta\gamma}\,K_1\!\left(r_{cD}\sqrt{z\eta\gamma}\right)a_{32}$$

$$= \gamma\sqrt{zf(z)}\,K_1\!\left(r_{cD}\sqrt{zf(z)}\right) \quad f_1 = -\frac{1}{C_D z^2 s + z} \tag{B.11}$$

Then the coefficients A_1, B_1 and B_2 will be obtained by solving equation (B.10). Further, the bottom hole pressure p_{wD} can be calculated by:

$$p_{wD} = A_1\!\left[I_0\!\left(\sqrt{z\eta\gamma}\right) - s\sqrt{z\eta\gamma}\,I_1\!\left(\sqrt{z\eta\gamma}\right)\ \right]$$
$$+ B_1\!\left[K_0\!\left(\sqrt{z\eta\gamma}\right) + s\sqrt{z\eta\gamma}\,K_1\!\left(\sqrt{z\eta\gamma}\right)\right] \tag{B.12}$$

References

Al-Otaibi, A.M., Wu, Y.-S., 2001. Transient behavior and analysis of non-darcy flow in porous and fractured reservoirs according to the barree and conway model, In: S.P.E. Western, Regional Meeting. Anaheim, California, USA doi: 10.2118/133533-MS.

Arbogast, T., Gomez, M.S.M., 2009. A discretization and multigrid solver for a Darcy–Stokes system of three dimensional vuggy porous media. Comput. Geosci. 13, 331–348.

Arbogast, T., Lehr, H.L., 2006. Homogenization of a Darcy–Stokes system modeling vuggy porous media. Comput. Geosci. 10, 291–302.

Barenblatt, G.I., Zheltov, I.P., Kochina, I.N., 1960. Basic concepts in the theory of seepage of homogeneous liquids in fissured rocks [strata]. J. Appl. Math. Mech. 24, 1286–1303.

Barree, R.D., Conway, M., 2009. Multiphase non-Darcy flow in proppant packs. SPE Prod. Oper. 24, 257–268.

Barree, R.D., Conway, M.W., 2004. Beyond beta factors: a complete model for Darcy, Forchheimer, and trans-Forchheimer flow in porous media, in: SPE Annual Technical Conference and Exhibition.

Camacho-Velazquez, R., Vasquez-Cruz, M., Castrejon-Aivar, R., Arana-Ortiz, V., 2005. Pressure-transient and decline-curve behavior in naturally fractured vuggy carbonate reservoirs. SPE Reserv. Eval. Eng. 8, 95–112.

Cheng, Q., Xiong, W., Gao, S.-S., Liu, H.-X., 2009. Channeling model of non-steady flow from matrix to insular cavity. Spec. Oil Gas Reserv. vol.16, pp. 53–54,81.

Edwards, D.A., Shapiro, M., Bar-Yoseph, P., Shapira, M., 1990. The influence of Reynolds number upon the apparent permeability of spatially periodic arrays of cylinders. Phys. Fluids A Fluid Dyn. 2, 45–55.

Evans, R.D., Hudson, C.S., Greenlee, J.E., 1987. The effect of an immobile liquid saturation on the non-Darcy flow coefficient in porous media. SPE Prod. Eng. 2, 331–338.

Forchheimer, P., 1901. Wasserbewegung durch boden. Z. Ver. Dtsch. Ing. 45, 1782–1788.

Gulbransen, A.F., Hauge, V.L., Lie, K.-A., 2010. A multiscale mixed finite-element method for vuggy and naturally-fractured reservoirs. SPE J. 15, 395–403.

Hu, X.-Y., Quan, L.-S., Qi, D.-S., Hou, J.-G., 2014. Features of cavern filling in fractured vuggy carbonate oil reservoirs, Tahe oilfield. Spec. Oil Gas Reserv. 21, 18–21.

Huang, H.-Y., Ayoub, J.A., 2008. Applicability of the Forchheimer equation for non-Darcy flow in porous media. SPE J. 13, 112–122.

Huang, Z.-Q., Yao, J., Li, Y.-J., Wang, C.-C., Lv, X.-R., 2011. Numerical calculation of equivalent permeability tensor for fractured vuggy porous media based on homogenization theory. Commun. Comput. Phys. 9, 180–204.

Huang, Z.-Q., Yao, J., Li, Y.-J., Wang, C.-C., Lv, X.-R., 2010. Permeability analysis of fractured vuggy porous media based on homogenization theory. Sci. China Technol. Sci. 53, 839–847.

Huang, Z.-Q., Yao, J., Wang, Y.-Y., 2013. An efficient numerical model for immiscible two-phase flow in fractured karst reservoirs. Commun. Comput. Phys. 13, 540–558.

Jia, Y.-L., Fan, X.-Y., Nie, R.-S., Huang, Q.-H., Jia, Y.-L., 2013. Flow modeling of well test analysis for porous–vuggy carbonate reservoirs. Transp. Porous Media 97, 253–279.

Kang, Z.-J., Li, J.-L., Zhang, D.-L., Wu, Y.-C., Zhang, J., 2005. Percolation characteristics of fractured-vuggy carbonate reservoir in Tahe oilfield. Oil Gas Geol. 26, 634–640.

Lai, B.-T., Miskimins, J.L., Wu, Y.-S., 2012. Non-Darcy porous-media flow according to the barree and conway model: laboratory and numerical-modeling. Stud. SPE J. 17, 70–79.

Li, L., 2013. Well Test Analysis Based on a New Model of High-velocity Non-Darcy Fluid Flow. J. Southwest Pet. Univ. Technol. Ed. vol. 35, pp. 99–105.

Li, Y., 2013. The theory and method for development of carbonate fractured-cavity

reservoirs in Tahe Oilfield. Acta Pet. Sin. 34, 115–121.

Li, Y., 2012. Ordovician carbonate fracture-cavity reservoirs identification and quantitative characterization in Tahe Oilfield. J. China Univ. Pet. Ed. Nat. Sci. 36, 1–7.

Liu, H., Wang, X., 2012. Pressure Response Characteristics in Large Scale Cavity Type Reservoir. J. Southwest Pet. Univ. Technol. Ed. vol. 34, pp. 94–99.

Liu, Y.-F., Liu, J.-C H, J. Z.-L., L, Z.-P., X, 2014. Well Test Curve Characteristic and Reservoir evaluation for Vuggy Carbonate Reservoirs. Sci. Tech. Engrg. vol. 14, pp. 121-126.

Lopez-Hernandez, H.D., 2007. Experimental analysis and macroscopic and pore-level flow simulations to compare non-darcy flow models in porous media. Colorado School of Mines.

Peng, X.-L., Du, Z.-M., Liang, B.-S., Qi, Z.-L., 2009. Darcy-stokes streamline simulation for the tahe-fractured reservoir with cavities. SPE J. 14, 543–552.

Popov, P., Efendiev, Y., Qin, G., 2009a. Multiscale modeling and simulations of flows in naturally fractured karst reservoirs. Commun. Comput. Phys. 6, 162–184.

Popov, P., Qin, G., Bi, L.-F., Efendiev, Y., Kang, Z.-J., Li, J.-L., 2009b. Multiphysics and multiscale methods for modeling fluid flow through naturally fractured carbonate karst reservoirs. SPE Reserv. Eval. Eng. 12, 218–231.

Ranjith, P.G., Viete, D.R., 2011. Applicability of the cubic law for non-Darcian fracture flow. J. Pet. Sci. Eng. 78, 321–327.

Stehfest, H., 1970. Algorithm 368: Numerical inversion of Laplace transforms. Commun. ACM 13, 47–49.

Wang, L., Wang, X.-D., Luo, E.-H., Wang, J.-L., 2014. Analytical modeling of flow behavior for wormholes in naturally fractured–vuggy porous media. Transp. Porous Media 105, 539–558.

Warren, J.E., Root, P.J., 1963. The behavior of naturally fractured reservoirs. Soc. Pet. Eng. J. 3, 245–255.

Wu, Y.-S., 2001. Non-Darcy displacement of immiscible fluids in porous media. Water Resour. Res. 37, 2943–2950.

Wu, Y.-S., Di, Y., Kang, Z., Fakcharoenphol, P., 2011a. A multiple-continuum model for simulating single-phase and multiphase flow in naturally fractured vuggy reservoirs. J. Pet. Sci. Eng. 78, 13–22.

Wu, Y.-S., Lai, B., Miskimins, J.L., Fakcharoenphol, P., Di, Y., 2011b. Analysis of multiphase non-Darcy flow in porous media. Transp. Porous Media 88, 205–223.

Yang, F., Wang, X.-H., Liu, H., 2011. Well test interpretation model for wells drilled in cavity of fractured vuggy carbonate reservoirs. Chin. J. Hydrodyn. 26, 278–283.

Yang, J., Yao, J., Wang, Z., 2005. Study of pressure-transient characteristic for triple-medium composite reservoirs. J. Hydrodyn. (Ser. A) 20, 418–425.

Yao, J., Huang, Z.-Q., Li, Y.-J., Wang, C.-C., Lv, X.-R., 2010. Discrete Fracture-Vug Network Model for Modeling Fluid Flow in Fractured Vuggy Porous Media, in: International Oil and Gas Conference and Exhibition in China.

Ye, Z.-H., Chen, D., Wang, J.-G., 2014. Evaluation of the non-Darcy effect in coalbed methane production. Fuel 121, 1–10.

Zhang, F., Yang, D.-Y., 2014a. Determination of minimum permeability plateau and characteristic length in porous media with non-Darcy flow behavior. J. Pet. Sci. Eng. 119, 8–16. http://dx.doi.org/10.1016/j.petrol.2014.04.018.

Zhang, F., Yang, D.-Y.T., 2014b. Determination of fracture conductivity in tight formations with non-darcy flow behavior. SPE J. 19, 34–44.

Zhang, F.-X., Chen, F.-F., Peng, J.-X., Jia, Y.-L., Lei, S.-L., Yang, X.-T., Yang, J.-J., 2009. A well test model for wells drilled in big-size cavity of naturally fractured vuggy carbonate reservoirs. Acta Pet. Sin. 30, 912–915.

Zhang, W.-B., Jin, Q., Xu, S.-Y., Tian, F., Cui, J.-J., 2012. Paleo-cavern filling characteristics and hydrocarbon reservoir implication in the Ordovician outcrops in northern Tarim Basin. Spec. Oil Gas. Reserv. 19, 50–54.